Angular and Seasonal Variation of Spectral Surface Reflectance Ratios: Implications for the Remote Sensing of Aerosol Over Land

Lorraine A. Remer, Andrew E. Wald, and Yoram J. Kaufman

***Abstract*—We obtain valuable information on the angular and seasonal variability of surface reflectance using a hand-held spectrometer from a light aircraft. The data is used to test a procedure that allows us to estimate visible surface reflectance from the longer wavelength 2.1 μm channel (mid-IR). Estimating or avoiding surface reflectance in the visible is a vital first step in most algorithms that retrieve aerosol optical thickness over land targets. The data indicate that specular reflection found when viewing targets from the forward direction can severely corrupt the relationships between the visible and 2.1 μm reflectance that were derived from nadir data. There is a month by month variation in the ratios between the visible and the mid-IR, weakly correlated to the Normalized Difference Vegetation Index (NDVI). If specular reflection is not avoided, the errors resulting from estimating surface reflectance from the mid-IR exceed the acceptable limit of $\Delta\rho \sim 0.01$ in roughly 40% of the cases, using the current algorithm. This is reduced to 25% of the cases if specular reflection is avoided.**

I. Introduction

When viewed from space, the striking difference between land and ocean surfaces is the uniformity of the ocean and the large spatial variability of the land. The extreme variability of reflectance from the land surface hinders the remote sensing of aerosol over land. One exception is the contrast reduction technique, in which the effect of aerosol in reducing the apparent variability of the surface reflectance is used to determine the change in the aerosol optical thickness ([12]). While there have been successful operational satellite retrievals of aerosol over the comparatively uniform ocean surface ([6]), attempts at an operational algorithm over land has eluded us. A few specific cases using advanced very high resolution radiometer (AVHRR) ([16]) have been successful. Likewise aerosol indices derived from total ozone mapping spectrometer (TOMS) and polarization and directionality of Earth reflectances (POLDER) provide qualitative or experimental aerosol information over land surfaces ([3], [4]). Still, we have been missing a quantitative, operational aerosol product over land.

One of the fundamental advances of the new moderate resolution imaging spectroradiometer (MODIS) sensor will be the regular retrieval of a quantitative aerosol product over land surfaces ([9], [1]). MODIS has this capability due to the inclusion of mid-infrared channels, especially the 2.1 μm band. The reflectance in the mid-IR passes through the obstructing aerosol, which permits us to characterize the surface reflectance. Hence, we can identify the dark surface pixels [8].

TABLE I
Dates and Times of each Flight, Whether Angular Information was Recorded, the Aerosol Optical Thickness at 670 nm (τ_{670}) During the Flight, the Solar Zenith Angle (θ_o) at the Time of the Flight, and the Mean Normalized Difference Vegetation Index (NDVI). Flights are Arranged in Seasonal Progression but Span Two Years

Date	Time of Takeoff	Angles Noted	τ_{670}	θ_o	NDVI
March 12, 1997	10:10 EST	Yes	0.10	46°	0.45
April 22, 1996	8:15 EST	Yes	0.10	51°	0.53
May 22, 1996	12:35 EST	No	0.20	23°	0.82
July 30, 1997	13:05 EST	No	0.05	32°	0.81
October 16, 1996	12:45 EST	Yes	0.15	51°	0.56

In previous work, Kaufman *et al.* [10] establish the relationships between the visible and mid-IR channels as

$$\rho_{red} = 0.50\rho_{2.1} \tag{1a}$$

$$\rho_{blue} = 0.25\rho_{2.1}. \tag{1b}$$

These relationships were derived from data collected mostly from the United States' east coast in July 1993 using high altitude spectral images, airborne visible-IR imaging spectrometer (AVIRIS) and Landsat thematic mapper (TM). Both sensors view the Earth's surface from the nadir direction only. Equations (1a) and (1b) were tested using independent data collected by other means, including a subset of the data presented in this study [9], [10], [1]. The results of the testing showed that the relationships in (1a) and (1b) were adequate to estimate visible surface reflectance and derive aerosol optical thickness to within the specified theoretical error bounds. However, the testing was performed on a limited data base of mostly high altitude sensors, at nadir view and during one month in the seasonal growing season.

In this study, we analyze data collected from a sensor aboard a low flying aircraft over Charles County, MD (38° 30′ N, 77° 05′ W). The low altitude eliminates the need to derive surface reflectance from high altitude apparent reflectance. The data are collected for off-nadir views, and the analysis emphasizes possible disruption to (1a) and (1b) from angular effects. By repeating measurements in the same location over several months,

Manuscript received October 1, 1999; revised March 30, 2000.

L. A. Remer and Y. J. Kaufman are with the Laboratory for Atmospheres, NASA/Goddard Space Flight Center, Greenbelt, MD 20771 USA (e-mail: remer@climate.gsfc.nasa.gov; kaufman@climate.gsfc.nasa.gov).

A. E. Wald is with the Science Applications International Corporation, Chantilly, VA 20151 USA (e-mail: andy@stillwater.saic.com).

Publisher Item Identifier S 0196-2892(01)01174-3.

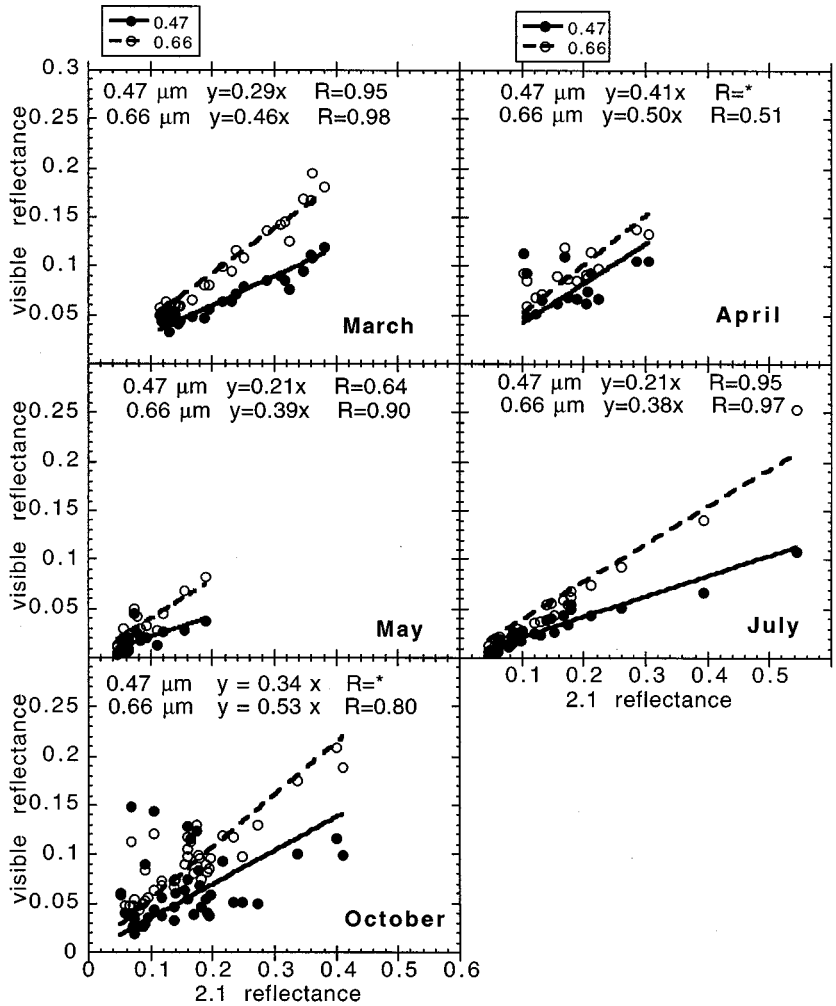

Fig. 1. Surface reflectance at 0.47 μm and 0.66 μm as a function of 2.1 μm surface reflectance for each of the flights described in Table I. Linear fits and correlation coefficient are shown. $R = *$ indicates no correlation.

we also examine whether the relationships expressed in (1a) and (1b) hold during the progression of a typical growing season in a temperate climatic zone.

II. Experimental Design

We collected spectra of the ground using a handheld analytic spectral device (ASD) spectrometer while flying over various surface targets in a Cessna at an altitude of 300 m. The spectra span the range from 440 nm to 2500 nm. The spectral resolution is 3 nm in the range of 400–1000 nm and 10 nm for longer wavelengths. The field of view is 18° full field, corresponding to a spot size of ~100 m from a platform at 300 m above the ground. The instrument head was held by hand out of the window with a nominal view angle of 45°±10°. Five to ten spectra were taken of each target during an elapsed time of roughly 15 to 30 s. The targets were of homogeneous surface type, 600–1000-m wide. The data were checked for spurious incursions into the field of view, and improper spectra were discarded. Then the remaining spectra were averaged for each

TABLE II
Ratios of $\rho_{0.47}/\rho_{2.1}$ (Top) and $\rho_{0.67}/\rho_{2.1}$ (Bottom) and Correlation Coefficients for all Targets, Targets Excluding Marshes, Swamps, and Estuaries, only Forest Targets, and Targets of all Surface Types but no Forward Scattering Views

Month	All Targets		No Marsh		Only Forest		No Forward	
	ratio	R	ratio	R	ratio	R	ratio	R
March	0.29	0.95	0.29	0.95	0.30	0.69	0.29	0.96
April	0.41	-	0.41	-	0.43	-	0.36	0.83
May	0.21	0.64	0.19	0.85	0.16	0.52	No angles	
July	0.21	0.95	0.21	0.95	0.20	0.71	No angles	
October	0.34	-	0.32	-	0.44	-	0.29	0.79

Month	All Targets		No Marsh		Only Forest		No Forward	
	ratio	R	ratio	R	ratio	R	ratio	R
March	0.46	0.98	0.46	0.98	0.42	0.97	0.46	0.98
April	0.50	0.51	0.50	0.51	0.51	-	0.47	0.90
May	0.39	0.90	0.35	0.91	0.23	0.71	No angles	
July	0.38	0.97	0.39	0.97	0.28	0.93	No angles	
October	0.53	0.80	0.51	0.88	0.56	0.46	0.50	0.96

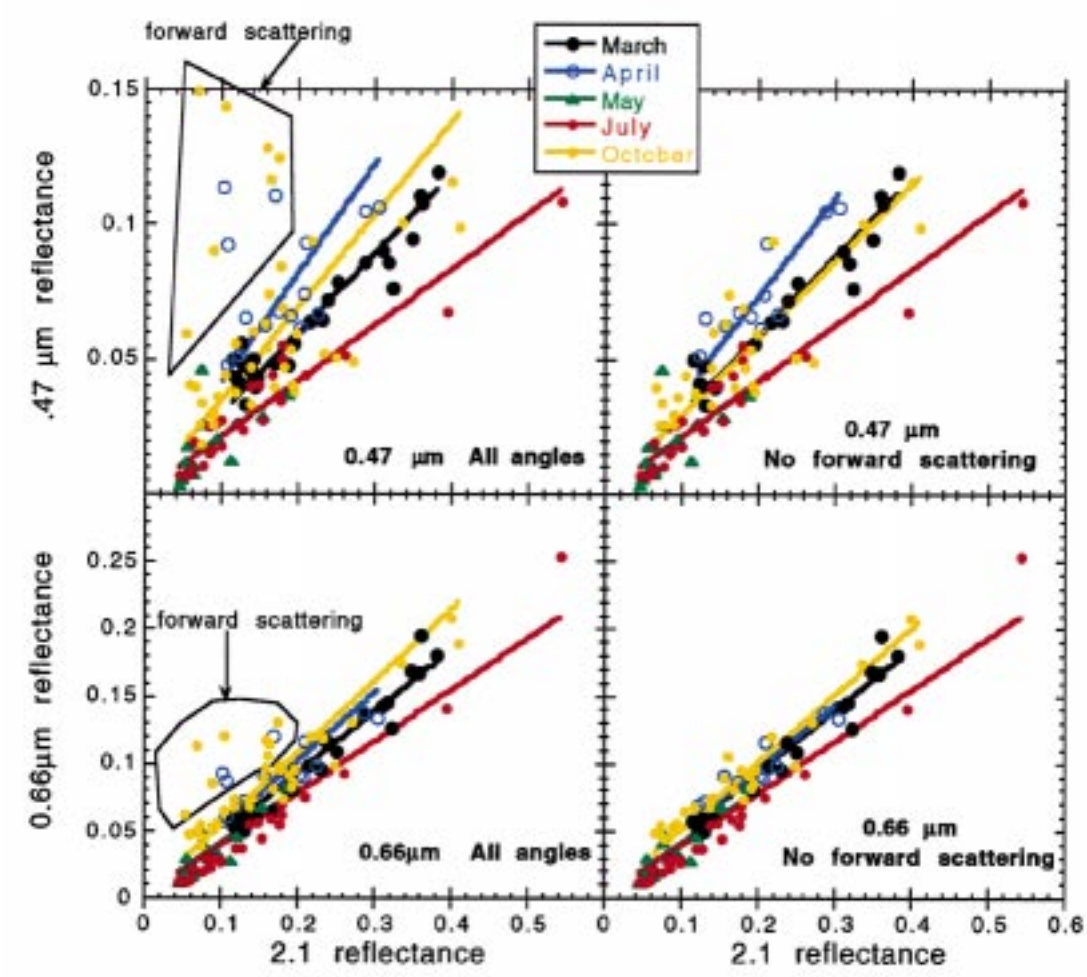

Fig. 2. (Top) Surface reflectance for 0.47 μm and (bottom) 0.66 μm as a function of 2.1 μm surface reflectance with all flights plotted on the same axes. The targets viewed from the forward scattering direction are indicated and removed from the plots on the right-hand side. Slopes and correlation coefficients are given in Table II.

target. We used a spectral square transmission function to calculate the reflectance in each MODIS band. In this study, we compare the ratios between different MODIS bands. These ratios were calculated from channels of a given spectrum. All channels were taken simultaneously at the same view angle.

The instrument was used in reflectance mode in which the radiance is normalized by baseline values taken of a white barium sulfate plate. White plate measurements were made immediately before boarding the aircraft. Flight duration was typically 1 h, and flight days were chosen to correspond to days of low optical thickness and homogeneous sky (Table I). In this way, sky conditions remained unchanged during the flight. Atmospheric correction based on the 6 s radiative transfer code ([16]) is applied to the data. The correction accounts for Rayleigh scattering, downwelling radiation, and spherical albedo. Because we were flying close to the ground and on relatively clean days, the correction is slight.

The five flights over a two-year period (Table I) span the natural vegetative seasonal cycle in the mid-Atlantic region. We revisited the same targets or similar targets on each flight and thus have a spectral record of the changing surface reflectance of surfaces ranging from deciduous forests to crop land to marshes and pasture. During the flights, we noted the surface type of

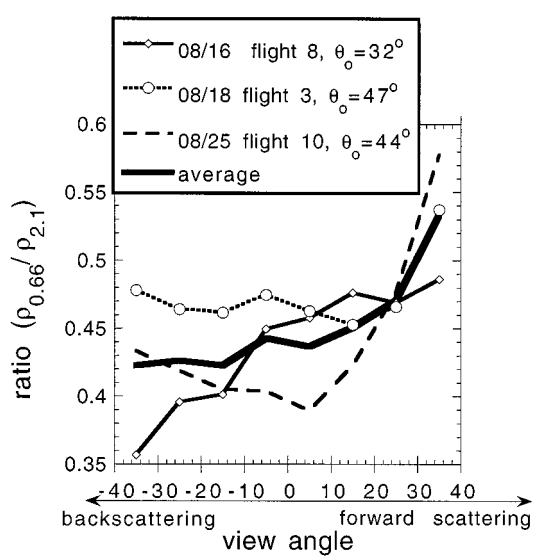

Fig. 3. Spectral surface reflectance ratio between the 0.66 μm and 2.1 μm channels, derived from atmospherically corrected MODIS airborne simulator apparent reflectances. Three flight lines and the average of the three are plotted. Solar zenith angle (θ_o) of each flight line is indicated. Scan of each flight was in the principal plane of the sun. Backscattering view angles are negative.

each target and the approximate viewing geometry, either forward, backward, or perpendicular to the principal plane. On two flights (May 1996 and July 1997), the solar zenith angle was too small to cast sufficient shadows on the ground for us to make a determination of the approximate azimuth of our viewing geometry.

III. Angular Dependence

The ratios between the visible and mid-IR developed from mostly nadir measurements in [10] are expected to hold better for the backward scattering direction than for the forward scattering direction. As the viewing angle of the target approaches specular reflection, the spectral signature of the reflectance lessens. This occurs because the specularly reflected sunlight originates at the interface between the air and the plant cuticular wax layer. The photons never enter the leaves, never interact with the liquid water or the pigments in the leaves, and therefore, are reflected off of the leaves with little spectral signature [15], [11]. In a plant canopy of randomly oriented leaves, specular reflectance can occur at all viewing geometries. However, plant canopies are not necessarily randomly oriented and previous studies [15], [11] have shown specular reflection to have preferential orientation to specific viewing angles, especially in the forward scattering direction when the sun is low in the sky.

A. Maryland Data

Fig. 1 shows the relationships between the visible and mid-IR channels from flights in different months. The data are also given in Table II. The slopes for the blue channel range from 0.21 to 0.41, as contrasted with the mean value of [10] of 0.25. In the red channel, the range is from 0.38 to 0.53, as compared to the [10] value of 0.50. However, some flights exhibit a strong correlation between the visible and mid-IR (March and July), while other flights do not (April and October).

The low correlation during the flights of April and October is mainly due to a subset of points identified in Fig. 2. These points represent targets that span the entire range of surface types found in the data set, including forest, corn stubble, and short grass. No standing water was noted in any of these targets. The flights exhibiting poor correlation occurred during the spring or fall when the vegetation was not yet fully leafed out or was already beginning to fade into senescence. However, the March flight, in another spring month with even less leaf area, exhibits a high correlation between mid-IR and visible reflectance.

The commonality of the points causing the low correlation in the April and October flights is that each of those targets was viewed in the forward scattering direction. Fig. 2 also shows the results of excluding all targets identified as being viewed from the forward scattering position. The results greatly increase the correlation in the April and October flights and bring the slopes of those lines closer to the expectations of (1a) and (1b). Table II gives the ratios and correlation coefficients for each flight, with and without targets viewed from the forward scattering direction. On the other hand, removal of the forward scattering points in the March flight data does not change the statistics for that flight.

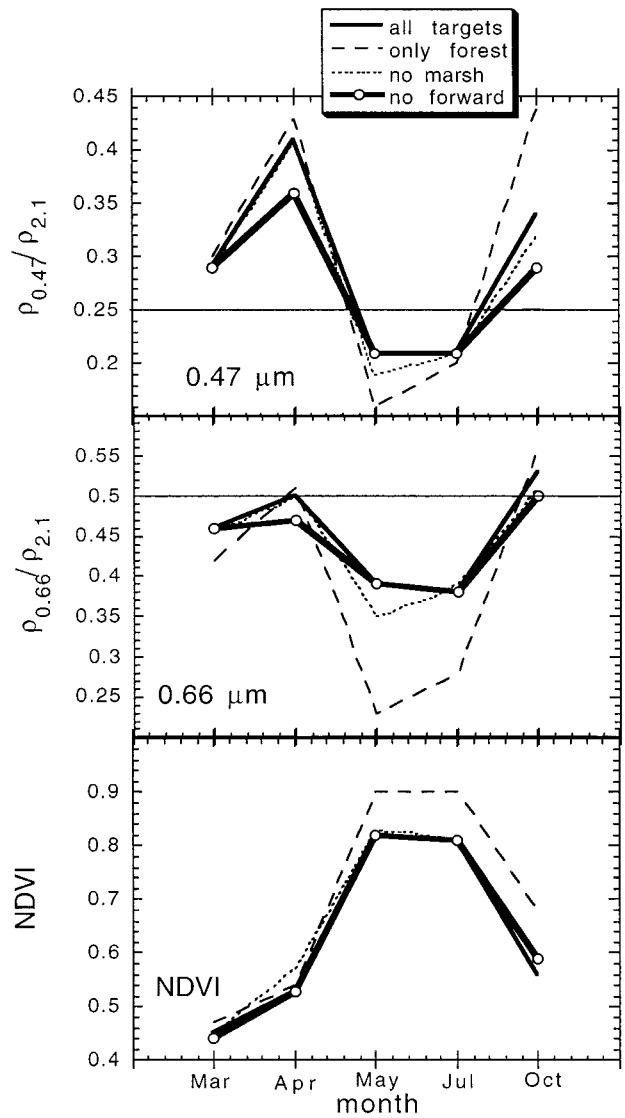

Fig. 4. Monthly mean ratios between the visible and 2.1 μm channel and the NDVI as a function of month. Shown are different subsets of the data including all targets (solid line), only forest targets (dashed line), all wetlands removed (dotted line), and all forward scattering targets removed (solid line with symbols).

Physically, we are seeing the effect of specular reflection from the leaf canopies. Like glint on water, specular reflection from a plant canopy causes the reflected radiation to lose its spectral signature [15] [11]. The ratios between the visible and mid-IR approach 1.0. Note the solar zenith angles from Table I. The April and October observations were made when the sun was lowest in the sky, even lower than the March flight. [11] shows that the specular component of the reflected light increases with increasing solar zenith angle, although there are some dependencies on canopy architecture. According to [11], the specular reflectance of the March flight with solar zenith angle of 46° would be less likely to dominate our measurements taken with view angle of 45° than would the April and October flights with solar zenith angle of 51°.

B. Brazilian Data

A different biome further illustrates the angular dependence of the spectral ratios. MODIS airborne simulator (MAS) data collected over Brazil during the Smoke, Clouds And Radiation—Brazil (SCAR-B) experiment ([7]) provides spectral-angular data of the tropical savanna. The data is not ideal for a study of surface reflectance because it is collected at high altitude and requires atmospheric correction. In order to reduce the severity of the atmospheric correction on the data, we restricted the data to flight lines in which the mean aerosol optical thickness at 670 nm was less than or equal to 0.15 and the variability across the image was less than or equal to 0.05. The images were corrected by using the 6 s code ([16]) on the apparent reflectances with inputs derived using the MODIS algorithm on nadir pixels.

In addition we required the scan direction to be within 20° of the principal plane. The MAS scans ±40°, which is slightly less than our pointing angle with the low flying, hand-held spectrometer. In order to find specular reflection in the data set, we will have to look for it at slightly lower solar zenith angles than we did with either the Maryland or Israeli data. We restrict solar zenith angles in the SCAR-B data set to 40±8°. The smoky conditions during SCAR-B eliminate much of the data for surface reflectance analysis. Adding the geometric criteria leaves us with only three flight lines to analyze. The data from each image was cloud screened and then sorted by view angle and averaged into bins representing 10° of view angle each. Each flight line represents over 4300 scan lines.

The spectral ratios of the SCAR-B MAS data as a function of view angle are plotted in Fig. 3. All three flight lines and the mean of the three show an increase in the ratios in the forward scattering direction, with the highest values occurring near the angle of specular reflection. The amount of increase of the ratios is less than what is seen in the Maryland data, but we expect that because the geometry is different. Even so, the ratios of (1a) and (1b) exhibit a clear angular dependence in which the ratios increase in the forward scattering direction near the angle of specular reflection.

Other angular measurements of the tropical savanna also point to the angular dependence of the ratio between visible and mid-IR surface reflectance. [14] describes a set of measurements of different surface types using the cloud absorption radiometer (CAR) in Brazil. The CAR permits the measurement of the full bidirectional reflectance of the surface at several different wavelengths. The CAR data show that the ratio between the surface reflectance of two visible channels and the 2.2 μm channel is dependent on viewing geometry, with the ratio increasing in the forward scattering direction [14], [2].

The basic agreement of the analysis resulting from these different biomes using different instrument techniques is strong evidence that the spectral ratios increase in the forward scattering direction. The results suggest specular reflection may introduce significant error to the MODIS aerosol retrieval algorithm. Therefore, we shall explore the improvement in remote sensing of aerosol over the land if the immediate region around the specular reflection is avoided, somewhat similar to the MODIS procedure used over the oceans [13].

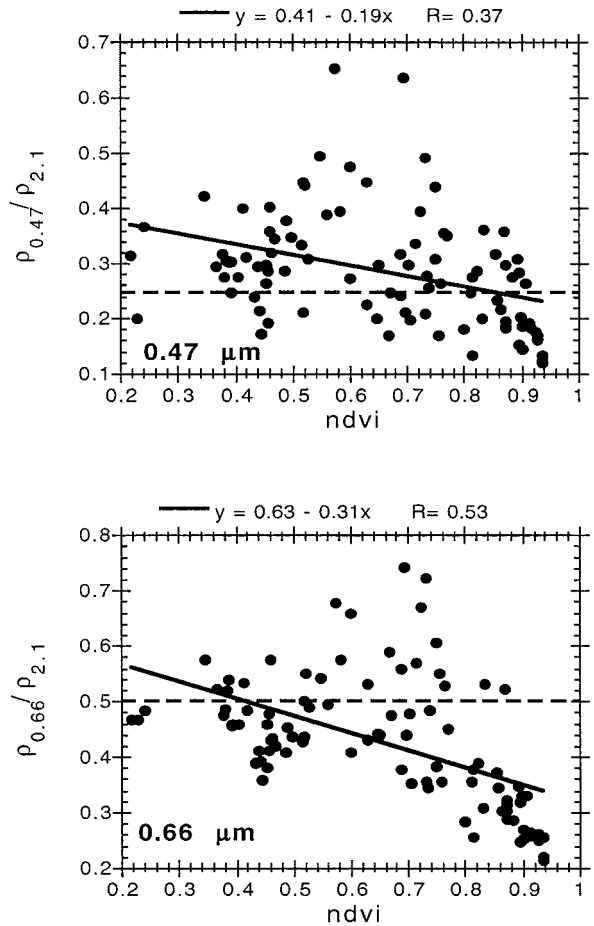

Fig. 5. Reflectance ratios for the (top) blue and (bottom) red as a function of the NDVI. The linear regression fits and correlation coefficients are given and depicted in the figure by a solid line. The expected values of 0.25 and 0.50, respectively, are shown by dashed lines. The data represent all targets from all flights with forward scattering targets removed.

IV. Seasonal and Surface Cover Dependence

The ratio between the visible and mid-IR surface reflectance exhibits a seasonal dependence. For both the blue and red channels the ratio decreases during the height of the growing season when the normalized difference vegetation index (NDVI) is at its peak. NDVI is defined as

$$\mathrm{NDVI} = (\rho_{0.87} - \rho_{0.66})/(\rho_{0.87} + \rho_{0.66}) \tag{2}$$

where $\rho_{0.87}$ is the surface reflectance at 0.87 μm, and $\rho_{0.66}$ is the surface reflectance at 0.66 μm. Fig. 4 shows the seasonal variation of the monthly mean values of the ratio for 1) all the targets; 2) all the targets except marshes; 3) only forest targets; and 4) all target types without forward scattering. Table II lists all ratios and all correlation coefficients.

The subset of "forest only" targets represent the targets of highest NDVI. As a group, these highly vegetated surfaces dramatically decrease the 0.66 μm ratio during the summer flights while increasing the 0.47 μm ratio during the October flight. In both cases, the forest subset moves the ratio further from the expected values of 0.50 and 0.25, respectively. The "forest only" subset represents the darkest targets with the lowest reflectance.

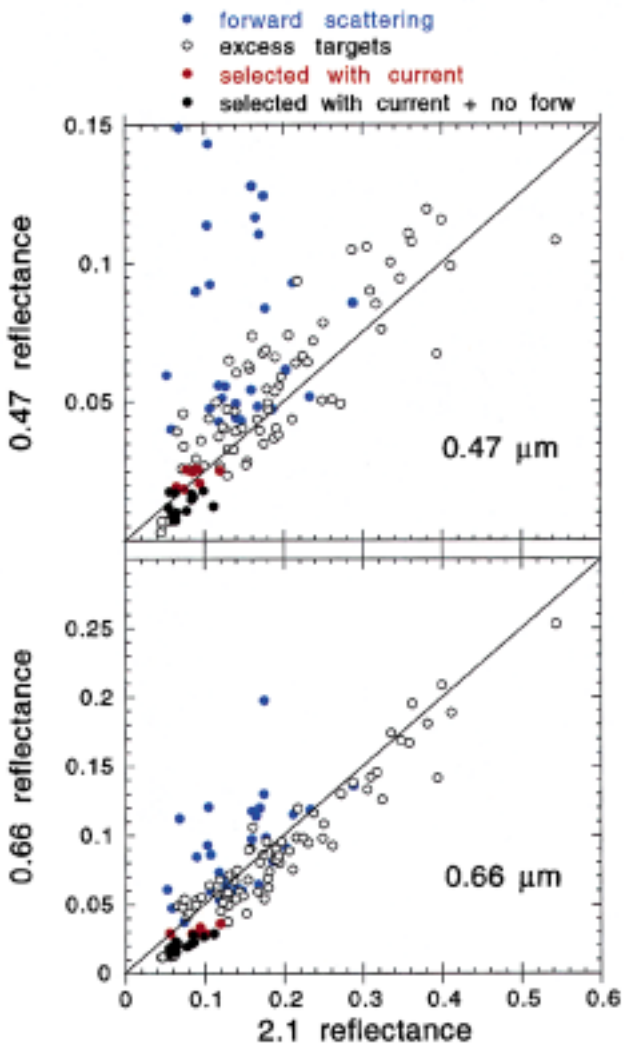

Fig. 6. Surface reflectance for (top) 0.47 μm and (bottom) 0.66 μm as a function of 2.1 μm surface reflectance with all flights plotted on the same axes. The targets viewed from the forward scattering direction are indicated by blue. Red points are those selected by current constraints, and black points are those selected when angular restrictions are added to the current constraints.

Because the forests are so dark [8], even though the percentage error in estimating visible reflectances will be large, the absolute error of applying (1a) and (1b) will be small.

Seasonal changes in reflectance spectra from plant canopies are well known and form the basis of the many vegetation indices, including NDVI. These vegetation indices are based on ratios between the visible part of the spectra where vegetation is dark and the near infrared part (0.87 μm) where vegetation is bright. The ratios introduced in (1a) and (1b) are not vegetation indices in that they are ratios between the visible (dark vegetation) and the mid-IR (2.1 μm) where vegetation is also dark. We expect seasonal changes in vegetation indices that are ratios between dark and bright parts of the spectrum. However, seasonal variability in ratios of the visible and mid-IR, both which are dark parts of the spectrum [(1a) and (1b)], as seen in Fig. 4, were not anticipated.

The sensitivity of the (1a) and (1b) ratios to NDVI is shown in Fig. 5 for the data from all flights combined. All forward scattering targets have been eliminated. Ratios decrease as NDVI increases, especially at 0.66 μm. However, the scatter in the relationships is large. The variability in visible to mid-IR ratios is due to deviations in the correlation between chlorophyll and liquid water in plant leaves, in canopy structure variations that alter shadowing patterns and in canopy background brightness. NDVI is sensitive to some, but not all of these factors and therefore, the weak correlation and scatter in Fig. 5 results.

Although Fig. 5 shows only a weak dependence between the spectral ratios and NDVI, there is still important information in the plot. The highest values of NDVI in Fig. 5 contribute the most to the decreasing trend in the correlation. This suggests that knowledge of the target NDVI may indeed be useful in modifying the coefficients of (1a) and (1b) in some circumstances. For example, in regions of extremely dark, dense vegetation where NDVI exceeds 0.85, it may be preferable to decrease the coefficient at 0.66 μm. The primary difficulty will be obtaining an atmospherically corrected NDVI. Atmospheric correction to retrieve surface properties from satellite observations requires knowledge of the aerosol optical thickness. Knowledge of aerosol optical thickness from a satellite requires knowledge of surface properties. Breaking through this circular dependence makes inclusion of NDVI criteria in the retrieval algorithm difficult. Using clear sky composite values may be the answer. The suggested relationship between the ratios and the vegetation index in this data set needs to be further examined in similar data collected in other regions of the world before the global algorithm can be modified.

V. Errors in Estimating Surface Reflectance

What are the errors in estimating visible surface reflectance using (1a) and (1b) for this data set? This question must be posed in context of the intended application. The purpose of estimating surface reflectance using (1a) and (1b) is to provide the basis for the remote sensing of aerosol over land. The remote sensing method is inherently a "dark target" method. (1a) and (1b) is not indiscriminately applied to each and every pixel observed by the satellite. Instead, there is an order of operation that was developed to minimize contamination and errors. The algorithm proceeds as follows.

- All pixels in a 10 km $\times$ 10 km grid box are grouped together for analysis. The MODIS 2.1 μm channel has a 500 m spatial resolution. Therefore, each analysis grouping includes up to 400 cloud free pixels.
- Only dark pixels, those pixels with $\rho_{2.1} < \rho_{\text{cutoff}}$, are included in the analysis. Currently, MODIS uses a cascade of cutoffs: $\rho_{\text{cutoff}} = 0.05$, 0.10, and 0.15. We shall test the last cutoff in this study.
- A filter is applied to the *visible* reflectance of remaining pixels. The brightest 60% as well as the darkest 10% measured in terms of the pixels' visible reflectance are discarded. We refer to this as the 10–40% filter. This filter is an operational check to eliminate clouds accidentally left unmasked, cloud shadows or other unexpected contamination in the procedure.
- Equations (1a) and (1b) are applied to each of the remaining pixels, visible reflectance is estimated, and the aerosol optical thickness retrieved.

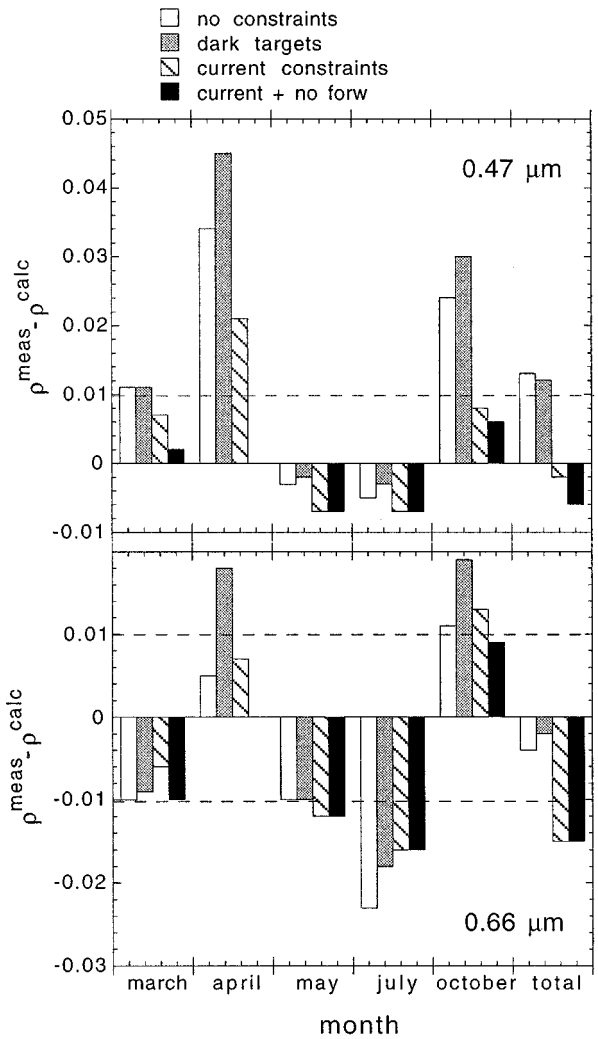

Fig. 7. Error defined as $\rho_\lambda^{\rm meas} - \rho_\lambda^{\rm calc}$ for $\lambda = 0.47\ \mu$m and 0.66 μm as a function of month for different combinations of pixel selection. No constraints indicates all pixels were included. Dark targets indicates that only targets with $\rho_{2.1} < 0.15$ are included. Current restraints indicate that both the dark target criterion and a filter that eliminates the 10% darkest targets and the 60% brightest targets are imposed. "No forw" indicates that all forward scattering targets were removed before the filter was applied. The last "month" plotted is actually a combination of all the targets from all five flights.

If there are less than 40 pixels that survive such a selection process, then no aerosol retrieval is attempted for that 10 km $\times$ 10 km square.

We apply (1a) and (1b) to our data set, flight by flight, for different combinations of constraints and selection processes. We include in this test a constraint on forward scattering. Forward scattering targets are removed at the time the 0.15 cutoff selects the dark targets, before the 10–40% filter is applied. In each month of our data, we assume that the targets represent the different pixels encountered in a 10 km square. A major difference between our testing procedure in this study and actual situations to be encountered by MODIS is our lack of pixels. While MODIS analysis will include up to 400 pixels in cloud-free conditions, we observed as few as 15 targets on one of our flights. In actuality, each of our flights contains fewer targets than the minimum necessary for the algorithm to proceed. Nonetheless, these are the available data, and we proceed with the testing in order to see how imposing the different constraints affects the error in estimating visible reflectance.

TABLE III
ERROR ANALYSIS BY MONTH AND FOR TOTAL COMBINED DATA SET

		March	April	May	July	October	Total
No constraints	N	27	15	18	25	40	125
	error 0.47	0.011	0.034	-0.003	-0.005	0.024	0.013
	error 0.66	-0.010	0.005	-0.010	-0.023	0.011	-0.004
Dark targets. (0.15 cutoff)	N	13	5	16	16	18	68
	error 0.47	0.011	0.045	-0.002	-0.003	0.030	0.012
	error 0.66	-0.009	0.018	-0.010	-0.018	0.019	-0.002
Current constraints (0.15 cutoff and 10-40% filter)	N	4	2	5	5	6	20
	error 0.47	0.014	0.021	-0.007	-0.007	0.008	-0.002
	error 0.66	-0.006	0.007	-0.012	-0.016	0.013	-0.015
Current constraints and angular restrictions	N	2	0	Angles not noted.		4	16
	error 0.47	0.002				0.006	-0.006
	error 0.66	-0.010		Same as current constraints		0.009	-0.015
0.15 cutoff and angular restrictions, but no 10-40% filter	N	6	1	16	16	15	53
	error 0.47	0.010	0.032	-0.002	-0.003	0.023	0.006
	error 0.66	-0.009	0.005	-0.010	-0.018	0.014	-0.005
10-40% filter and angular restrictions but no cutoff	N	5	2	5	8	8	28
	error 0.47	0.012	0.025	-0.007	-0.006	0.006	-0.001
	error 0.66	-0.009	-0.005	-0.012	-0.018	0.007	-0.010

Fig. 6 illustrates the severity of imposing the different constraints. This figure shows the combined data set of all five flights. The targets remaining after the current constraints are imposed are represented by the combination of red and filled black points. Except for the darkest 10% of the targets, which do not pass the 10–40% filter, the surviving points are the darkest targets. The blue points are those targets viewed from the forward scattering direction. When these points are eliminated first, before imposing the current constraints, the surviving targets are reduced to the set of filled black points only.

Error is defined as $\rho_\lambda^{\rm meas} - \rho_\lambda^{\rm calc}$, where $\rho_\lambda^{\rm meas}$ is the observed reflectance at wavelength λ, and $\rho_\lambda^{\rm calc}$ is the reflectance calculated from (1a) and (1b) at the same wavelength. Fig. 7 shows and Table III lists the average error due to imposing different sets of constraints on our different data sets. Because each month contains so few targets compared to the anticipated 400 pixels from the MODIS analysis, we add a sixth data set in which we combine all months to create a data base of 125 pixels. The combined data base spanning the growing season is an artificial conglomerate and may introduce a higher degree of variability of land surface reflectance than would typically be available in a 10 km $\times$ 10 km square. The combined data set is labeled as "total" in Fig. 7 and Table III. The label "no constraints" refers to the application of (1a) and (1b) for all the targets, all the angles, with no imposed dark target threshold and no 10–40% filter. The label "dark targets" refers to imposing a cutoff of $\rho_{2.1} < 0.15$ in order to include only the darkest targets. The label "current constraints" refer to those pixels that survive the $\rho_{2.1} < 0.15$ cutoff and the 10–40% filter, but have no restriction on the view angle. Finally the category "current + no forw" is the most re-

strictive and eliminates all forward scattering targets in addition to imposing the current constraints.

We must estimate the surface reflectance in the visible to within ~0.01 in order to retrieve optical thickness to within ~0.10. Imposing no constraints at all on the data introduces unacceptable errors in half the cases. Simply restricting the analysis to dark targets reduces the error in July, but not enough to bring it down to acceptable levels at 0.66 μm, and in April and October, "dark targets" actually increases the error. Passing the dark targets through the 10–40% filter improves the situation. The "current restraints," which include both the $\rho_{2.1} < 0.15$ cutoff and the 10–40% filter on the visible reflectance, results in 40% of the cases having unacceptable errors. However, once the forward scattering targets are removed from the "current restraints" category, only 25% of the cases introduce unacceptable levels of error. Part of this improvement is due to the elimination of all pixels from the April flight.

Although the selection process reduces the error in estimating surface reflectance from the mid-IR, unacceptable error occurs in 25% of the cases. These cases are estimates in the red channel for the May and July flights and the combined data set of all sites. The combined data is dominated by the May/July data for the darkest targets. The lower panel of Fig. 6 illustrates the reason for the error. The surviving targets designated by filled black points, all fall below the diagonal line representing (1a) and (1b). These very dark, dense vegetated surfaces at the height of the growing season do not conform to the expected spectral ratio. The reason is unclear.

VI. Discussion and Conclusions

We obtained valuable information on the angular and seasonal variability of surface reflectance using a hand-held spectrometer on a light aircraft. In general, our data support the hypothesis of a strong correlation between surface reflectance in the visible and mid-IR. We discovered that the correlation is most robust when the view angle is not in the forward scattering direction. As the geometry approaches specular reflection, the surface reflectance becomes less spectrally dependent, and the relationships between spectral bands break down. This angular dependence identified in the Maryland data set was supported by atmospherically corrected data collected over the tropical savanna by a radiometer aboard a high altitude aircraft.

The ratios between spectral bands follows a seasonal pattern and are weakly correlated with surface characteristics as quantified by NDVI. The ratios are lowest during the prime growing season when NDVI is highest. During May and July, the months of highest NDVI, the ratios in the red channel are half of what was expected. The errors occur regardless of view angle. The large errors in July at 0.66 μm are puzzling. The formulation data set used to derive the original relationships between spectral bands was constructed from July data in similar locations to the area we observed for this study. We would have expected the spectral ratios of the July data in the current data set to most closely resemble the original formulation. However, even the original data set included specific surface types of very low ratios for the 0.66 channel. The current data falls within the scatter of the original measurements.

Using the ratio method to determine surface reflectance in the visible is a viable method to retrieve aerosol optical thickness over land. However, a series of constraints must be imposed in order to capture the darkest targets in the scene. Removing forward scattering pixels will help reduce errors significantly if the view angle approaches specular reflection.

Retrieval of aerosol optical thickness over land continues to be a difficult problem. Understanding the angular dependencies of the retrieval and possibly restricting retrieval near the specular reflection direction will enhance the overall accuracy of the final MODIS aerosol product. Taking advantage of the weak relationship between NDVI and the surface reflectance ratios will need further exploration. A comprehensive data set of similar spectrometer data from a low flying airplane taken in the nadir direction was collected over a desert transition zone in Israel. We expect analysis of these data from an alternative biome will help to complete our picture of the effect of NDVI on estimating surface reflectance in the visible and will eventually lead to an even more accurate MODIS aerosol product.

Acknowledgment

The authors would like to thank G. Wen and C. Gatebe for reviewing the manuscript and offering very helpful comments. They would also like to thank Beacon Aviation, Clinton, MD, and S. Provoncha, L. Coleman, and J. Cager for their assistance in collecting the data.

References

[1] D. A. Chu, Y. J. Kaufman, L. A. Remer, and B. N. Holben, "Remote sensing of smoke from MODIS airborne simulator during the SCAR-B experiment," *J. Geophys. Res.*, vol. 103, 1998.

[2] C. K. Gatebe, M. D. King, S. C. Tsay, Q. Ji, G. T. Arnold, and J. Y. Li, "Sensitivity of off-nadir zenith angles to correlation between visible and near-infrared reflectance for use in remote sensing of aerosol over land," *IEEE Trans. Geosci. Remote Sensing*, to be published.

[3] J. R. Herman, P. K. Bhartia, O. Torres, C. Hsu, C. Seftor, and E. Celarier, "Global distribution of UV-absorbing aerosols from Nimbus 7/TOMS data," *J. Geophys. Res.*, vol. 102, pp. 16 911–16 922, 1997.

[4] M. Herman, J. L. Deuzé, C. Devaux, P. Goloub, F. M. Bréon, and D. Tanré, "Remote sensing of aerosols over land surfaces including polarization measurements and application to POLDER measurements," *J. Geophys. Res.*, vol. 102, pp. 17 039–17 049, 1997.

[5] A. R. Huete and C. J. Tucker, "Investigation of soil influences in AVHRR vegetation imagery," *Int. J. Remote Sensing*, 1990.

[6] R. B. Husar, L. L. Stowe, and J. M. Prospero, "Characterization of tropospheric aerosols over the oceans with the NOAA advanced very high resolution radiometer optical thickness operational product," *J. Geophys. Res.*, vol. 102, pp. 16 889–16 910, 1997.

[7] Y. J. Kaufman, P. V. Hobbs, V. W. J. H. Kirchoff, P. Artaxo, L. A. Remer, B. N. Holben, M. D. King, D. E. Ward, E. M. Prins, K. M. Longo, L. F. Mattos, C. A. Nobre, A. M. Thompson, J. F. Gleason, and S. A. Christopher, "The smoke cloud and radiation experiment in Brazil (SCAR-B)," *J. Geophys. Res.*, vol. 103, no. 31, pp. 783–31 808, 1998.

[8] Y. J. Kaufman and L. A. Remer, "Detection of forests using mid-IR reflectance: An application for aerosol studies," *IEEE Trans. Geosci. Remote Sensing*, vol. 32, pp. 672–683, Sept. 1994.

[9] Y. J. Kaufman, D. Tanré, L. A. Remer, E. Vermote, A. Chu, and B. N. Holben, "Operational remote sensing of tropospheric aerosol over land from EOS moderate resolution imaging spectroradiometer," *J. Geophys. Res.*, vol. 102, pp. 17 051–17 067, 1997.

[10] Y. J. Kaufman, A. E. Wald, L. A. Remer, B.-C. Gao, R.-R. Li, and L. Flynn, "The MODIS 2.1 μm Channel—Correlation with visible reflectance for use in remote sensing of aerosol," *IEEE Trans. Geosci. Remote Sensing*, vol. 35, pp. 1286–1298, 1997.

[11] G. Rondeaux and V. C. Vanderbilt, "Specularly modified vegetation indices to estimate photosynthetic activity," *Int. J. Remote Sensing*, vol. 14, pp. 1815–1823, 1992.

[12] D. Tanré, P. Y. Deschamps, C. Devaux, and M. Herman, "Estimation of Saharan aerosol optical thickness from blurring effects in thematic mapper data," *J. Geophys. Res.*, vol. 92, pp. 15 955–15 964, 1988.

[13] D. Tanré, Y. J. Kaufman, M. Herman, and S. Mattoo, "Remote sensing of aerosol properties over oceans using the MODIS/EOS spectral radiances," *J. Geophys. Res.*, vol. 102, pp. 16 971–16988, 1997.

[14] S.-C. Tsay, M. D. King, T. Arnold, and J. Y. Li, "Airborne spectral measurements of surface anisotropy during SCAR-B," *J. Geophys. Res.*, vol. 103, no. 31, pp. 943–953, 1998.

[15] V. C. Vanderbilt and K. J. De Venecia, "Specular, diffuse and polarized imagery of an oat canopy," *IEEE Trans. Geosci. Remote Sensing*, vol. 26, pp. 451–462, 1988.

[16] E. F. Vermote, D. Tanré, J. L. Deuzé, M. Herman, and J. Morcrette, "Second simulation of the satellite signal in the solar spectrum: An overview," *IEEE Trans. Geosci. Remote Sensing*, vol. 35, pp. 675–686, May 1997.

Lorraine A. Remer received the B.S. and Ph.D. degrees in atmospheric science from the University of California, Davis, and the M.S. in oceanography from the Scripps Institution of Oceanography, University of California, San Diego.

She has been with NASA/Goddard Space Flight Center since 1991. From 1988 to 1991, she was with Science Systems and Applications, Inc., when she became a Civil Servant. She is an Associate Member of the EOS-MODIS Science Team and a Member of the Global Aerosol Climatology Project Science Team. Her current research interests are the climatic effects and remote sensing of atmospheric aerosol. She has been involved in several field campaigns including the Smoke/Sulfate, Cloud and Radiation (SCAR) experiments, the Tropospheric Aerosol Radiative Forcing Observational Experiment (TARFOX), the Israeli Desert Transition Zone Experiment, and the Puerto Rico Dust Experiment (PRiDE).

Andrew E. Wald received the B.S. and M.S. in optics from the University of Rochester, Rochester, NY, in 1987, and the M.A. and Ph.D. degrees in physics and the in earth and planetary sciences, respectively, from The Johns Hopkins University, Baltimore, MD, in 1990 and 1994, respectively.

He was a Postdoctoral Researcher with the College of Oceanic and Atmospheric Sciences, Oregon State University, Corvallis, working on cloud remote sensing, and had an NRC Postdoctoral Fellowship with NASA/Goddard Space Flight Center, Greenbelt, MD, on remote sensing of aerosols, biomass burning, vegetation, and mineralogy. He is currently Senior Staff Scientist, Science Applications Internation Corp. (SAIC), Chantilly, VA.

Yoram J. Kaufman received the B.Sc. and M.Sc. degrees in physics from the Technion–Israeli Institute of Technology, Haifa, Israel, and the Ph.D. from the Tel-Aviv University, Tel Aviv, Israel.

He was with NASA/Goddard Space Flight Center in 1979 on an NRC Fellowship Award. He is currently a Senior Atmospheric Scientist with NASA Goddard Space Flight Center, Greenbelt, MD, the Project Scientist of the Earth Observing System first satellite: EOS-Terra, launched in December 1999, and a Member of the EOS-MODIS Science Team. His present work includes theoretical and experimental research in atmospheric radiative transfer and remote sensing. It includes remote sensing of aerosol, its interaction with clouds and radiation, and impact on climate with emphasis on biomass burning in the tropics. He conducted the Smoke/Sulfate, Clouds And Radiation (SCAR) field experiments in Brazil and the U.S. to characterize aerosol properties and their effect on clouds and radiation. He has over 120 refereed publications.

Dr. Kaufman has received several NASA/GSFC awards.